

Focused ion beam preparation of samples for X-ray nanotomography

Jeffrey J. Lombardo,^a Roger A. Ristau,^b William M. Harris^a and Wilson K. S. Chiu^{a*}

Received 21 December 2011

Accepted 15 June 2012

^aDepartment of Mechanical Engineering, University of Connecticut, 191 Auditorium Road, Storrs, CT 06269-3139, USA, and ^bInstitute of Material Science, University of Connecticut, 97 North Eagleville Road, Storrs, CT 06269-3136, USA. E-mail: wchiu@enr.uconn.edu

The preparation of hard material samples with the necessary size and shape is critical to successful material analysis. X-ray nanotomography requires that samples are sufficiently thin for X-rays to pass through the sample during rotation for tomography. One method for producing samples that fit the criteria for X-ray nanotomography is focused ion beam/scanning electron microscopy (FIB/SEM) which uses a focused beam of ions to selectively mill around a region of interest and then utilizes a micromanipulator to remove the milled-out sample from the bulk material and mount it on a sample holder. In this article the process for preparing X-ray nanotomography samples in multiple shapes and sizes is discussed. Additionally, solid-oxide fuel cell anode samples prepared through the FIB/SEM technique underwent volume-independence studies for multiple properties such as volume fraction, average particle size, tortuosity and contiguity to observe the characteristics of FIB/SEM samples in X-ray nanotomography.

© 2012 International Union of Crystallography
Printed in Singapore – all rights reserved

Keywords: X-ray nanotomography; focused ion beam; solid-oxide fuel cell; sample preparation.

1. Introduction

Synchrotron-based X-ray nanotomography has been proven to be an effective non-destructive method for studying the microstructure of hard materials with sub-40 nm resolution such as lanthanum strontium manganite (LSM), nickel, yttria-stabilized zirconia (YSZ) (Izzo *et al.*, 2008), amorphous aluminosilicate cements (Provis *et al.*, 2011) and SiO₂-coated Pt₉₀Ir₁₀ tips (Rose *et al.*, 2011). This technique exploits the different rates of X-ray absorption by different materials which then appear as contrast difference in transmission images of the sample. However, to discern the detailed location of different materials, it is necessary to rotate the sample and take images at multiple angles of rotation to discern between contrast changes due to different materials, and changes that arise from different sample thickness, a process that is known as tomography (Herman, 2009). In addition to exploiting contrast differences using one X-ray energy level, a synchrotron-based X-ray source allows for the variation of the irradiating X-ray energy allowing one to probe an atomic transition for a specific material in the sample. For example, Ni has a *K* transition near 8333 eV, which appears as a rapid increase in absorption for Ni samples as the X-ray energy is scanned across the edge. This fact can be exploited to identify elements of interest and with careful analysis it can also be used to discern between different oxides of a material (Nelson *et al.*, 2011a).

Adequate preparation of samples for study in X-ray nanotomography is crucial for obtaining clear, accurate and unambiguous results. An ideal sample should be thin enough to allow a significant proportion of X-rays to transmit through the sample, while thick enough that different phases and materials absorb enough X-rays to produce sufficient contrast for differentiating between them. For common solid-oxide fuel cell (SOFC) materials such as LSM/YSZ ceramic composite and Ni/YSZ cermet, this thickness was found to be of the order of 10 µm when imaged at 8350 eV (Nelson *et al.*, 2011b; Nelson *et al.*, 2012). In studies of amorphous aluminosilicate cements and fly-ash (Provis *et al.*, 2011), a 7.5 µm-diameter fly-ash particle coated with aluminosilicate geopolymer gel was successfully imaged at 10 keV, while a Pt₉₀Ir₁₀ tip was able to provide absorption contrast for nanotomography even when a sample less than 1 µm thick was imaged at 778 eV (Rose *et al.*, 2011). Additionally the sample needs to be large enough that the data obtained from the sample is representative of the material as a whole. The sample also needs to possess an acceptable thickness throughout rotation about an axis so that enough signal can be obtained at multiple angles to allow for tomographic reconstruction. Finally, the sample should be small enough that the entirety of the sample remains within the transmission X-ray microscope's field of view and depth of field. For the transmission X-ray microscope used in this study, a 25 µm ×

25 μm field of view was used with a depth of field of $\sim 25 \mu\text{m}$, but these values are highly dependent on the optics used in the microscope.

Many sample preparation techniques have been developed to thin samples including, but not limited to, microtomy (Quintana, 1997), dimple grinding (Bruemmer & Thomas, 2001), ion milling (Chew & Cullis, 1987) and electrochemical thinning and polishing (Sabinina & Gutakovsky, 1992). All of these techniques have been used with great success with a variety of instruments including transmission electron microscopes (TEMs), and all of these techniques can be used to thin a sample to varying degrees of precision and thickness. However, attempting to form a second or third dimension at the micrometer or nanometer scale is increasingly difficult or not possible with many techniques, and, even if additional dimensions are thinned, handling and moving the sample can be difficult. One technique that has the potential to address these issues is focused ion beam/scanning electron microscopy (FIB/SEM).

Focused ion beam microscopy uses a beam of focused ions, typically gallium, to selectively mill regions of a sample (Young *et al.*, 1998; Giannuzzi & Stevie, 1999; Li *et al.*, 2006) in order to create three-dimensional samples at the micrometer or nanometer scale. The ions can also be used to obtain an image of the sample as well by taking advantage of secondary electrons produced during the milling process. In many systems a scanning electron microscope is also attached to provide finer image resolution. In addition to milling and imaging capabilities many systems also have the ability to deposit materials such as Pt by decomposing a carrier gas with the ion beam over the region where the material is desired. Finally, a built-in computer-controlled micromanipulator coupled with a tilt, translational and rotational stage allows the FIB system to maneuver material and remove a sample and position it onto a sample holder.

In this article the preparation of X-ray nanotomography samples was performed using a FIB/SEM system to make samples in multiple shapes and sizes using a modification of the commonly used 'lift-out' procedure (Giannuzzi & Stevie, 1999; Li *et al.*, 2006; Munroe, 2009; Wo *et al.*, 2009; Budiman *et al.*, 2010). In the lift-out technique, a sample is milled out from a bulk material using the focused ion beam and lifted out from the bulk material using a micromanipulator and is then attached to a substrate such as a TEM grid by way of ion-deposited Pt or another material. Because this technique is typically used for transmission electron microscopy preparation, the produced samples tend to be electron transparent. This means that the sample is almost always less than 1 μm in thickness, or even thinner for denser materials. Additionally, because the imaging occurs at one angle or over a small variation of angles, samples traditionally tend to be thinned only in one direction. Both of these characteristics are ill suited to X-ray nanotomography analysis because sub-1 μm -thick samples will not in general provide adequate absorption contrast, and the one dimension of thinning does not typically provide acceptable path lengths for X-ray transmission as the sample is rotated throughout 180°. For this reason it is

important to modify the procedure in such a manner that more X-ray contrast is achieved by use of a thicker sample, and that the sample is in such a geometry that the X-ray path length is uniform for all angles of rotation. For Ni/YSZ SOFC anode samples a 10 μm X-ray path length was found to provide sufficient X-ray contrast. For this reason the standard lift-out procedure was modified to accommodate these requirements, mainly through the creation of a cylindrical sample. Additional shapes were also then proposed that allow for different specifications to be met.

Upon completion of the modified lift-out procedure on an Ni/YSZ SOFC anode, the prepared sample was studied using synchrotron-based X-ray nanotomography and multiple properties of the sample were measured including volume fraction, average particle size, tortuosity and contiguity. It should be noted that while synchrotron-based X-ray nanotomography was the basis of this study owing to its high illumination intensity, X-ray energy tunability and sub-50 nm resolution, it is also possible to utilize the sample preparation technique outlined in this article to create samples for laboratory-based transmission X-ray tomography.

2. Sample preparation

To prepare a sample for use in X-ray nanotomography, the bulk material was attached to a SEM specimen mount using carbon tape and coated with Au/Pd using a Polaron E5100 SEM Coating Unit. Next the sample was loaded into a FEI Strata 400 DualBeam FIB/SEM system. Upon focusing and bringing the sample to the eucentric height, the desired final geometry was planned out using simple two-dimensional shapes to remove material that will dictate the length and width of the final sample while using the milling time to control the final height of the sample. For X-ray nanotomography, two shapes were most commonly used, one shape being a rectangular prism and the other being a cylinder. The rectangular prism is ideal for obtaining single-angle transmission images and can also be used for X-ray fluorescence study if the sample is sufficiently thin, while the cylindrical sample is more ideal for tomography. Typically the dimensions of a sample are such that the length and width of the sample will fit into the field of view for the X-ray nanotomography system which is typically around 40 μm or less, but ensuring that it is large enough to obtain a representative amount of sample for analysis. The thickness, which is the amount of sample that the X-ray beam must pass through from the X-ray source to the detector, is typically made such that 10–90% of the incident X-rays are absorbed by the sample for all of the given operating conditions. To determine the optimal X-ray beam path length when the material composition and structure is well known, an estimate can be made using the CXRO (Gullikson, 2010) calculator for X-ray transmission based on the work of Henke *et al.* (1993). In situations where the composition and/or structure are unknown, a series of samples with different thicknesses may be created to determine optimal sample size. Tomography can also be performed on the rectangular samples, even if the sample width is too large

to obtain sufficient X-ray counts for angles that align with the width of the sample. This is achieved by reducing the angles of tomography from 180° to a smaller rotation. However, care must be taken as the quality of the tomographic reconstruction will deteriorate as the number of angles are restricted (Hanson & Wecksung, 1983; Hanson, 1982). The second shape, the cylinder, is generally the preferred geometry for tomography because it allows a uniform maximum path length for X-rays throughout 180° of rotation, while also maximizing the volume of material that can be analyzed for any given maximum path length.

During the planning for the final shape, care must be taken to leave sufficient room for material to leave the crater surrounding the sample, a clear view of the base of the sample must be observable when the sample holder is tilted within the limits of the FIB system, and a balance must be struck between removing sufficient material to allow for the preceding requirements *versus* limiting the time it takes to make an individual sample. The technique for preparing a rectangular prism sample has been outlined in the literature (Giannuzzi & Stevie, 1999). The cylindrical shaped sample is less commonly seen in the literature as the uniform path length in rotation is not as important in many non-tomographic techniques. To create this shape, first the diameter of the cylinder was selected to produce the desired contrast in the X-ray nanotomography system, which as previously stated for LSM/YSZ and Ni/YSZ was $10\ \mu\text{m}$. Next the height of the sample was selected based on the field of view of the tomography system. From these two parameters a majority of the design can be set. To create a cylinder a series of concentric rings are milled out in series, beginning with the largest-diameter ring having a diameter (D) as outlined in equation (1) where θ is the desired tilt angle of the sample stage that will be used to cut off the cylinder sample as described below and shown in Fig. 2. Typically θ will be selected to be the angle between the ion beam and the electron beam for a given FIB system so that when cutting with the ion beam at θ to remove the cylinder from the bulk material one can view the progress of the cut from top of the sample as well. It should be noted that D is a suggested starting diameter; however, the actual desired outer diameter may change based on the material and system being used,

$$D = 2 \times \text{Desired sample height} \times \tan(\theta) + \text{Desired sample diameter}. \quad (1)$$

The starting ring, which is the ring with the largest diameter, should have an outer diameter equal to D and an inner diameter equal to the desired sample diameter plus $5\ \mu\text{m}$. The second ring is then milled after the first ring completes and shares the same inner diameter as the first circle but with an outer diameter that is smaller than the outer ring by $\sim 10\%$ of the difference in diameter between the largest ring and the cylinder diameter. The reason for this increment is that it was found that $\sim 10\%$ reduction in size per step allowed for sufficient clearance for sputtered material to leave the bottom of the milled crater, while not removing so much material as to

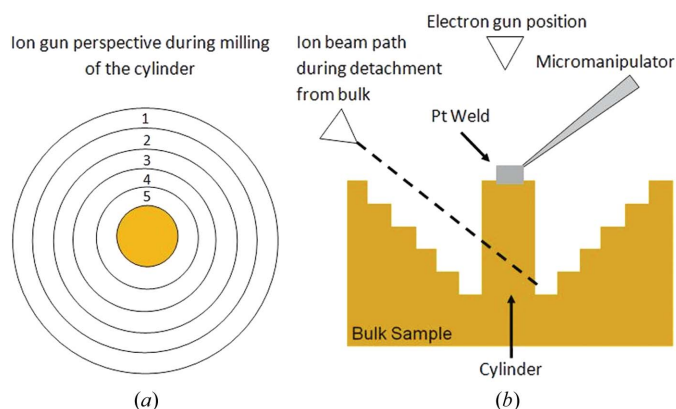


Figure 1
(a) Representation of the pattern used to create a cylindrical sample. Milling will take place in the numbered order with the final cylinder being shown in the shaded region. (b) Positioning of the system during cut-off and lift-out of the sample.

require a longer sample preparation time than necessary. This shrinking of the milling ring is demonstrated in Fig. 1(a), where the numbers on the rings represent the order in which they are milled. The staircase pattern also allows for viewing on the base of the sample when tilting the sample holder which is crucial for the detachment of the sample from the bulk material. The depth of the milling for each circle is generally kept uniform and is calculated such that the last ring will mill the crater immediately surrounding the cylinder down to the desired final height. The concentric milling of the rings is typically done under the higher beam currents allowable by the FIB system. For the FEI Strata 400 DualBeam system a current of $21\ \text{nA}$ at $30\ \text{kV}$ acceleration voltage was used. Once the concentric rings reach the base of the cylinder, another ring with the same dimensions as the final ring in the previous step is milled to a depth of $\sim 5\ \mu\text{m}$ to allow room for sputtered material that will be created in the following steps. At this point the excess $5\ \mu\text{m}$ added to the cylinder diameter is milled off using progressively lower beam currents, typically ending with a current of $2.8\ \text{nA}$ or lower when milling out the final surface. It should be noted that selecting the appropriate milling conditions near what will ultimately be the finished surfaces is important to reduce the damage caused to the sample by the ion beam. In TEM specimen preparation with FIB systems it has been observed that damage can occur to the sample due to ion beam interaction, up to tens of nanometers below the exposed surface. To reduce this damage on the milling surface, lower milling currents can be used to allow less spread in the ion beam, as was used in the method presented in this paper. Additionally, the accelerating voltage can be reduced to lower the energy available to the ions thus preventing them from penetrating as far into the sample. Other methods have also been proposed such as using gas-assisted etching, wet or dry etching and using broad ion-beam milling (Kato, 2004). However, because samples for X-ray nanotomography are thicker than TEM samples and X-ray nanotomography can provide measurements in the volume of a sample, the damage induced to the outer tens of nanometers of a sample can also be handled by discarding the data

collected from the damaged region. It should be noted that when studying the Ni/YSZ anode material an amorphous layer was found to reside in the outer few nanometers of the cylinder and is suspected to be caused by sample damage as well as redeposited material from the detachment process described below. Comparison of the structural properties of the same material studied in this article were also performed elsewhere and it was found that structural measurements from X-ray nanotomography using both FIB/SEM and traditional polishing sample preparation techniques compared within experimental uncertainty (Nelson *et al.*, 2011b).

Now that the cylinder has been milled to the desired diameter, it is necessary to detach the sample from the bulk material and move it to a substrate that will allow for easy handling of the sample while allowing for X-ray transmission to occur throughout the desired rotational angles. This is done by utilizing a built-in micromanipulator in the FIB system. First the sample is tilted such that the electron beam is facing the top of the ion-milled cylinder and the ion beam is tilted to the cylinder such that the cylinder base can be viewed with the ion beam as shown in Fig. 1(b). The micromanipulator is brought in and can be maneuvered such that it contacts the top of the cylinder, or if the surface of the cylinder will be very sensitive to damage or redeposition the micromanipulator can be attached to the side of the cylinder. Once the micromanipulator is maneuvered into the desired location it is attached to the sample with Pt deposited by the ion beam. For the Pt deposition an ion-beam acceleration voltage of 30 keV was used, and the ion beam current was adjusted depending on the size of the deposition region. For the $2\ \mu\text{m} \times 3\ \mu\text{m}$ area typically used for micromanipulator attachment a current of 93 pA was used leading to a flux of $15.5\ \text{pA}\ \mu\text{m}^{-2}$, but the optimal current rate will ultimately depend on the system used. Finally the ion beam is focused near the bottom of the cylinder and is used to cut the cylinder from the bulk sample. The cut must be high enough from the base of the cylinder so that when the cut passes through the cylinder and reaches the side furthest from the ion beam the cut is still occurring above the base of the cylinder, which is demonstrated in Fig. 1(b). If the cut is made too low, by the time it goes through the cylinder it will be cutting into the bulk sample and the cylinder will still be attached to the bulk material. Also, the width of the cut into the cylinder must be at least a few micrometers thick, depending on the material, because the cylinder is thick enough that material will start to redeposit near the cut entry and around the cylinder causing the sample to stay attached to the bulk material after the cut is complete. Once the cylinder is completely detached from the bulk material it should be lifted out from the crater. At this point the sample will be a cylinder with a triangular section on the bottom where the cut was made to remove the sample. This triangular portion can be removed through ion milling; however,

it will redeposit some of the material back onto the surface of the cylinder or it can be left on. Next the micromanipulator and sample are rotated and moved into position near an appropriate substrate. For the experiments that will be discussed later in this article a watch pin was used (Swiss Jewel Company SD-4D) as it was found to have a tip sufficiently sharp to mount a $10\ \mu\text{m}$ -diameter cylinder without having any of the substrate obscure X-ray transmission through the cylinder. The sample is then aligned and rotated using the electron beam for imaging such that the sample is flush with the surface of the pin. Next the ion beam is used at low imaging currents, and the sample is rotated again so that the sample is flush with the pin. This process is iterated until the sample appears to be well aligned using both beams. Next the sample is brought to the substrate using the slowest speed available on the micromanipulator until contact is made. Finally the base of the cylinder is attached to the substrate using Pt and then the micromanipulator is cut from the sample using the ion beam. At this point the sample is ready to be transported and mounted into an X-ray nanotomography system. SEM images showing the lift-out and mounting process are shown in Fig. 2. For Ni/YSZ SOFC anodes this entire process can take between 4 and 8 h, with roughly half the time spent milling out the $\sim 50000\ \mu\text{m}^3$ crater, and the other half used to remove the sample from the bulk material and to mount it on an appropriate substrate. For other materials a different cylinder size may be required owing to the material's X-ray absorption properties, and milling rates may be different depending on the sputter yield of the material under ion bombardment. The variation between sample preparation time will be most pronounced during the initial milling phase where the sputter yield can vary over an order of magnitude depending on the elements contained in the sample (Giannuzzi & Stevie, 2005).

In addition to the cylindrical shape, other shapes may be desired for different applications. The simplest of these shapes is the rectangular prism which can be made using a very similar approach to traditional TEM sample preparation as mentioned previously. The extra thickness typically used in X-ray absorption samples compared with TEM samples requires that some modification be made to the standard approach. Firstly, when milling into the bulk material, the craters on either side of the slab should be milled deeper than

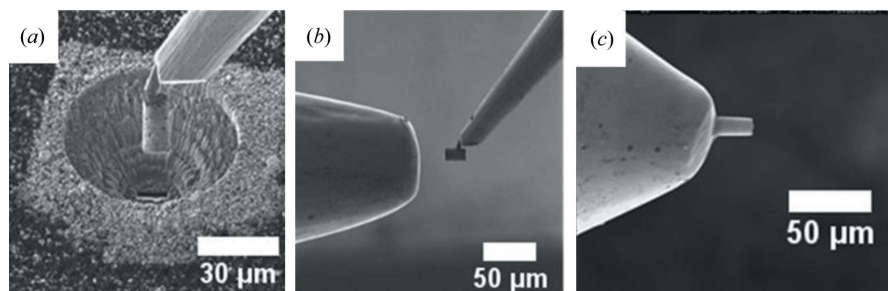


Figure 2

Demonstration of the lift out procedure. SEM images of (a) micromanipulator attachment and removal of the sample from the bulk, (b) positioning of the sample near the substrate, (c) attachment of the FIB cylinder to the substrate using Pt.

the desired sample height because the geometry of the detachment cut will cause the back side of the cut to be micrometers below the start of the cut. In addition, because of the larger thickness, it can be beneficial to start a detachment cut from one face of the rectangular sample and then rotate the sample 180° and create another detachment cut from the other side. This helps ensure that successful detachment occurs since the deeper cuts required to remove the thicker samples fill in as they go deep into the sample. This geometry does not typically work as well for tomography because of the wide variation in X-ray path length across rotation angles, but it can be used in single-angle X-ray absorption measurements. Additionally the rectangle can be thinned after mounting to ensure a clean surface by rotating the sample such that the thin edge of the rectangle is facing the ion beam and then milling the rectangle to the desired thickness. A wedge shape is also possible as a derivative of the rectangular shape. To create a wedge shape a rectangular sample is milled out in the bulk sample. Next the sample is tilted so a cut can be made into the rectangular sample such that a wedge will result (Fig. 3*a*). Once the desired angle is selected, the micro-manipulator should be attached to the sample at the final cutting angle and then the sample should be milled until it detaches. The wedge shape can be useful in X-ray nanotomography or X-ray fluorescence when the desired thickness of a sample is not known as it provides a continuous range of thicknesses. A cone can also be made using the FIB system from a cylindrical sample. To do this a cylindrical sample is made per previous instruction. Next a series of circular areas are milled out of the cylinder as demonstrated in Fig. 3*b*), with most ion beam dwell time near the outer surface of the cylinder and with little to no dwell time at the center of the cylinder. When milling occurs in this fashion the outer layers are milled down almost completely while the center is intact which approximates a conical shape. Cone samples are similar to wedge samples in that they can be used to determine the optimal sample thickness. However, a cone can be rotated while maintaining the same X-ray path length whereas a

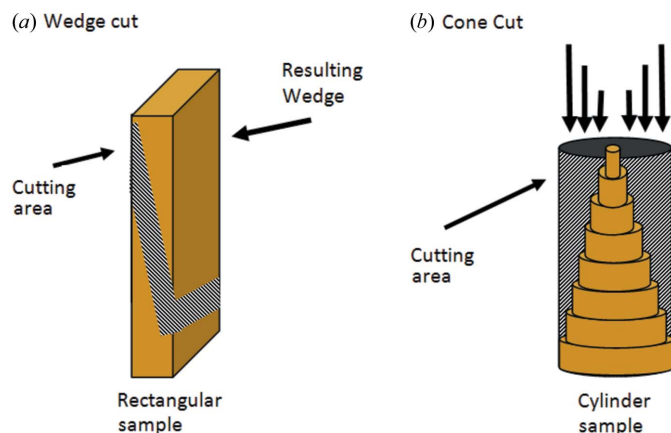


Figure 3
(*a*) Demonstration of the cutting area to produce a wedge-shaped sample.
(*b*) Illustration of how milling time varies as a function of radial position when producing a cone sample. The lengths of the vertical arrows indicate the relative milling time.

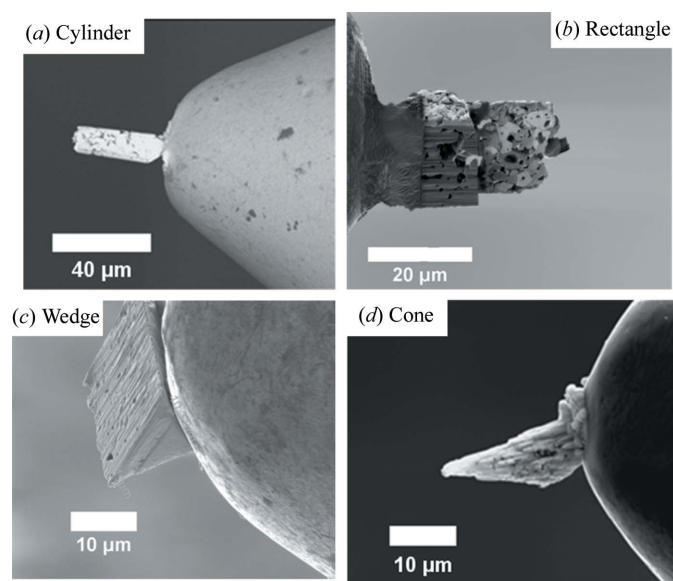


Figure 4
(*a*) FIB-produced cylinder 10 μm in diameter. (*b*) Rectangular sample thinned to 1 μm near the sample end. (*c*) Wedge sample tapering from 10 μm to 1 μm . (*d*) Cone sample with 10 μm base.

wedge cannot. Creation of cone-shape samples is also more difficult than the other shapes mentioned as porous features can cause uneven milling which will cause a rough surface. Examples of a FIB-produced cylinder, rectangle, wedge and cone are shown in Fig. 4.

3. Results and discussion

To demonstrate that FIB-produced samples are viable for study with X-ray nanotomography, a case study will be shown using a 10 μm -diameter cylinder produced using the FIB/SEM technique described in this article. X-ray nanotomography was performed at the Advanced Photon Source at Argonne National Laboratory (beamline 32-ID-C¹). 181 projection images were taken of the sample at 1° increments at 8356 eV. A previous study of X-ray nanotomography using SOFC cathodes has been compared with FIB/SEM serial sectioning (Nelson *et al.*, 2011*b*), and it was confirmed that structural properties of FIB/SEM-prepared samples measured using X-ray nanotomography are in good agreement with serial sectioning by FIB/SEM. Fig. 5 shows the sample used for volume-independence study, with a transmission image of the sample shown in Fig. 5(*a*) and a reconstructed cross section shown in Fig. 5(*b*). In Fig. 5(*b*) Ni is the bright white phase, YSZ is seen as the intermediate gray phase, and pore is shown as black. Volume-independence studies were performed using a 6.6 μm cube from the interior of the cylinder and the data were segmented and analyzed using previously developed codes and analysis (Grew *et al.*, 2010*a,b*; Nelson *et al.*, 2012).

Volume-independence studies were performed using progressively smaller volumes from the 6.6 μm region of study,

¹ Beamline 32-ID-B, C: Sector 32, Insertion Device Beamline, http://www.aps.anl.gov/Beamlines/Directory/showbeamline.php?beamline_id=84.

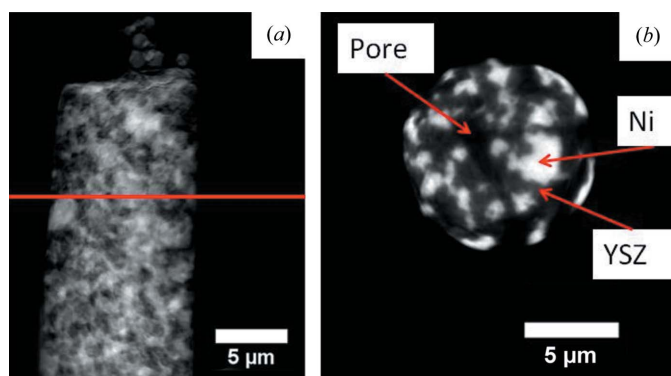


Figure 5
 (a) Transmission image of a 10 μm cylinder. The horizontal line denotes the location of the cross-sectional image. (b) Cross section of a 10 μm cylinder with Ni showing as white, YSZ showing as gray, and pore appearing as black.

with cubes of 6.6 μm, 5.3 μm, 4.0 μm, 2.7 μm and 1.3 μm on a side being used. These volume-independence studies observe how different properties of the material change depending on the volume selected, and are used to determine the minimum

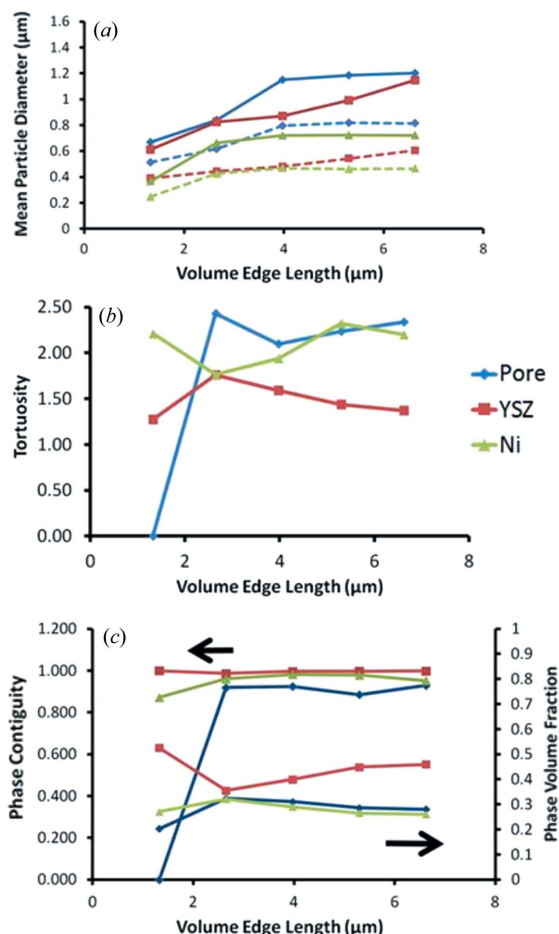


Figure 6
 Calculated properties for individual phases at multiple selected volume sizes. (a) Mean particle diameter. Solid lines: number-weighted; dashed lines: volume-weighted. (b) Tortuosity. (c) Phase contiguity (left) and phase volume fraction (right). Phase contiguity and tortuosity are 0 for pore in the 1.3 μm cube as the entire pore phase is isolated from the cube surface.

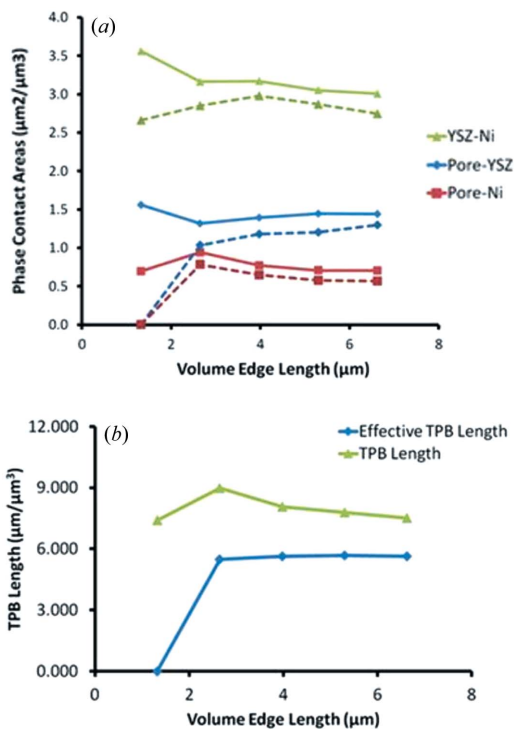


Figure 7
 Calculated values for properties involving more than one phase over multiple selected volume sizes. (a) Phase contact area. Solid lines: phase contact area; dashed lines: effective phase contact area. (b) TPB length. Effective phase contact area for pore-YSZ and pore-Ni and effective TPB length is 0 for the 1.3 μm region because the entire pore region is isolated for that selected volume.

size of material that needs to be studied in order to obtain representative results. A property was determined to be volume-independent if the property of interest did not change by more than 5% between two consecutive volume sizes. All cubes share the same center and look at progressively smaller regions of the initial volume. Each cube was analyzed to determine the volume fraction of each phase, the mean particle diameter weighted for both the total volume and the total number of particles, the tortuosity of each phase, and the contiguity of each phase (Fig. 6). Additionally, the contact area between phases, the contact area between contiguous phases (effective contact area), the triple-phase boundary length (TPB length) and the triple-phase boundary length between contiguous phases (effective TPB length) were also calculated and are shown in Fig. 7. From the studied parameters, phase contiguity and effective TPB length reached volume independence at a volume of 4.0 μm while volume fraction and phase contact area appeared to reach volume independence by 6.6 μm. Mean particle diameter using both forms of weighting, effective phase contact areas and TPB length still varied between the last two volume steps but appeared to be nearing volume independence. One of the reasons for the variability of the mean particle diameter, TPB length and the phase contact areas was the existence of several large particles in the YSZ phase which caused the mean particle diameter for YSZ to increase as the volume size increased, while pore and Ni remained fairly constant above

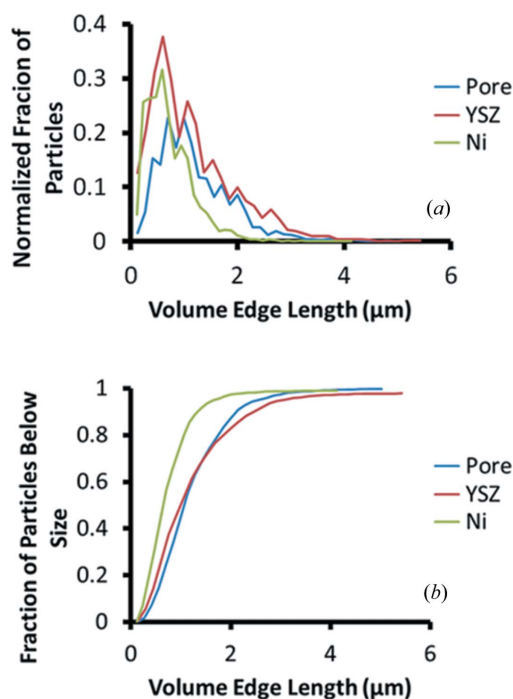


Figure 8

(a) Particle size distribution normalized by volume for the 6.6 μm volume.
 (b) Cumulative particle size distribution normalized by volume for the 6.6 μm volume.

the 4.0 μm volume. This also carried over into the effective phase contact areas where the contact areas involving YSZ still varied between the 5.3 μm and the 6.6 μm case. Tortuosity was still varying between the last two volume sizes for all three phases which suggests that 6.6 μm is not a large enough volume to claim volume independence for the sample studied.

Further analysis of the volume independence study and the particle size distributions in Fig. 8 shows physical properties of the material such as average particle diameter, volume fraction and contiguity appear to be independent of the selected volume if the analyzed volume edge length is at least twice the size of the largest particle in the set. In the case of YSZ, particles over 3.3 μm were present and caused fluctuation between the largest two volume sizes selected in the volume-independence study. Parameters that are a function of two or more phases in the material such as TPB length and phase contiguity were also independent if the volume edge length is twice the largest particle for each of the constituent phases. Again, one of the YSZ containing properties, the effective phase contact area for YSZ–Ni, still showed change at 6.6 μm because of the relatively large YSZ particles compared with the volume size. It should be noted that volume independence can be reached on a case-by-case basis even when the volume edge length is not twice the largest particle, but, for every case where a property was not independent, one of the constituent phases was found to have particles larger than half the volume edge length. Tortuosity does not show independence even when the volume is twice the size of the largest particles which may stem from the anisotropy of tortuosity (Grew *et al.*, 2010a) in the three principle directions of the selected volume causing additional variability.

4. Conclusions

This article presents an approach for fabricating samples for X-ray nanotomography using a FIB/SEM-based technique. This technique allows for samples to be created that are micrometer scale in all three dimensions, and can be fabricated in a variety of sizes and shapes depending on the application and the materials that compose the sample. Samples shaped as a cylinder, a rectangular prism, a wedge and a cone were all produced using this method, and many other shapes can be potentially made if the experimental needs warrant it. A case study was also presented to demonstrate that FIB/SEM samples can be successfully used in X-ray nanotomography and provide sufficiently large volumes to obtain volume independence for some properties, while properties such as tortuosity may require larger volumes to obtain volume-independent results.

We acknowledge financial support from the Energy Frontier Research Center on Science Based Nano Structure Design and Synthesis of Heterogeneous Functional Materials for Energy Systems (HeteroFoam Center) funded by the US Department of Energy, Office of Science, Office of Basic Energy Sciences (Award DE-SC0001061). The authors thank Jan Van Herle and his research group at École Polytechnique Fédérale de Lausanne for providing SOFC anode samples for analysis. X-ray nanotomography work was performed with Dr Steve Wang at the Advanced Photon Source supported by the US Department of Energy, Office of Science, Office of Basic Energy Sciences, under contract No. DE-AC02-06CH11357. We thank Dr John R. Izzo Jr and Dr George J. Nelson for assistance in performing X-ray tomography experiments.

References

- Bruemmer, S. M. & Thomas, L. E. (2001). *Surf. Interface Anal.* **31**, 571–581.
- Budiman, M., Hsu, E. M., Hauger, H. K. & Botton, G. A. (2010). *Appl. Phys. A*, **98**, 849–853.
- Chew, N. G. & Cullis, A. G. (1987). *Ultramicroscopy*, **23**, 175–198.
- Giannuzzi, L. A. & Stevie, F. A. (1999). *Micron*, **30**, 197–204.
- Giannuzzi, L. A. & Stevie, F. A. (2005). *Introduction to Focused Ion Beams*, 1st ed. Berlin: Springer.
- Grew, K. N., Peracchio, A. A. & Chiu, W. K. S. (2010b). *J. Power Sources*, **24**, 7943–7958.
- Grew, K. N., Peracchio, A. A., Joshi, A. S., Izzo, J. R. Jr & Chiu, W. K. S. (2010a). *J. Power Sources*, **24**, 7930–7942.
- Gullikson, E. (2010). *X-ray Interactions With Matter*, http://henke.lbl.gov/optical_constants/.
- Hanson, K. M. (1982). *Proc. Soc. Photo. Opt. Instrum. Eng.* **374**, 166–173.
- Hanson, K. M. & Wecksung, G. W. (1983). *J. Opt. Soc. Am.* **73**, 1501–1509.
- Henke, B. L., Gullikson, E. M. & Davis, J. C. (1993). *At. Data Nucl. Data Tables*, **54**, 181–342.
- Herman, G. T. (2009). *Fundamentals of Computerized Tomography: Image Reconstruction from Projection*, 2nd ed. Berlin: Springer.
- Izzo, J. R. Jr, Joshi, A. S., Grew, K. N., Chiu, W. K. S., Tkachuk, A., Wang, S. H. & Yun, W. (2008). *J. Electrochem. Soc.* **155**, 504–508.
- Kato, N. I. (2004). *J. Electron Microsc.* **53**, 451–458.
- Li, J., Malis, T. & Dionne, S. (2006). *Mater. Charact.* **57**, 64–70.

- Munroe, P. R. (2009). *Mater. Charact.* **60**, 2–13.
- Nelson, G. J., Grew, K. N., Izzo, J. R. Jr, Lombardo, J. J., Harris, W. M., Faie, A., Hessler-Wyser, A., Van herle, J., Wang, S., Chu, Y. S., Virkar, A. N. & Chiu, W. K. S. (2012). *Acta Mater.* **60**, 3491–3500.
- Nelson, G. J., Harris, W. M., Izzo, J. R. Jr, Grew, K. N., Chiu, W. K. S., Chu, Y. S., Yi, J., Andrews, J. C., Liu, Y. & Pianetta, P. (2011a). *Appl. Phys. Lett.* **98**, 197109.
- Nelson, G. J., Harris, W. M., Lombardo, J. J., Izzo, J. R. Jr, Chiu, W. K. S., Tanasini, P., Cantoni, M., Van herle, J., Comninellis, C., Andrews, J. C., Liu, Y., Pianetta, P. & Chu, Y. S. (2011b). *Electrochem. Commun.* **6**, 586–589.
- Provis, J. L., Rose, V., Winarski, R. P. & van Deventer, J. S. J. (2011). *Scr. Mater.* **65**, 315–319.
- Quintana, C. (1997). *Micron*, **28**, 217–219.
- Rose, V., Chien, T. Y., Hiller, J., Rosenmann, D. & Winarski, R. P. (2011). *Appl. Phys. Lett.* **99**, 173102.
- Sabinina, I. V. & Gutakovsky, A. K. (1992). *Ultramicroscopy*, **3–4**, 411–415.
- Wo, P. C., Munroe, P. R., Vasiliev, M., Xie, Z. H., Alameh, K. & Kotov, V. (2009). *Opt. Mater.* **32**, 315–322.
- Young, R. J., Carleson, P. D., Da, X., Hunt, T. & Walker, J. F. (1998). *Proceedings of the 24th International Symposium on Testing and Failure Analysis*, pp. 329–336. Materials Park: ASM International.